Azimuthal correlations of pions in relativistic heavy ion collisions at 1 GeV/nucl.

S. A. Bass[a,b], C. Hartnack[b,c], H. Stöcker[a] and W. Greiner[a]

[a]*Institut für Theoretische Physik der J. W. Goethe Universität*
Postfach 11 19 32, 60054 Frankfurt am Main, Germany
[b]*GSI Darmstadt, Postfach 11 05 52, 64220 Darmstadt, Germany*
[c]*Laboratoire de Physique Nucléaire, Nantes, France*

Abstract

Triple differential cross sections of pions in heavy ion collisions at 1 GeV/nucl. are studied with the IQMD model. After discussing general properties of Δ resonance and pion production we focus on azimuthal correlations: At projectile- and target-rapidities we observe an anticorrelation in the in-plane transverse momentum between pions and protons. At c.m.-rapidity, however, we find that high p_t pions are being preferentially emitted perpendicular to the event-plane. We investigate the causes of those correlations and their sensitivity on the density and momentum dependence of the real and imaginary part of the nucleon and pion optical potential.

I. INTRODUCTION

One of the main goals of the study of relativistic heavy ion collisions is the determination of the density and momentum dependence of the real and imaginary part of the nucleon (and other hadron) optical potential (often also termed nuclear equation of state) [1–7]. Its importance stretches well beyond nuclear physics and is of great importance for the formation of nuclear matter after the big bang, the behaviour of supernovae and neutron stars. It also is important for the quest for the quark-gluon plasma in heavy ion collisions.

An increasing number of observables which are accessible through heavy ion collisions has been found to be sensitive to the equation of state: Among the most prominent ones are collective flow effects such as the bounce–off of cold spectator matter *in* the reaction plane [8] and the squeeze–out of hot and compressed participant matter *perpendicular* to the reaction plane [9] as well as particle production [10–12]. The pion multiplicity was one of the first observables suggested to be sensitive to the nuclear equation of state [10–12]. This was motivating a strong experimental effort (4π analysis of streamer chamber events at the BEVALAC) [13–15]. However, the sensitivity of pion yields and spectra [16] on the equation of state is not very high [17,18] and therefore the attention shifted towards *subthreshold* production of mesons (e.g. kaons and η-mesons) [19–23].

New experimental 4π setups at two of the major heavy ion reasearch facilities, GSI (FOPI, KaoS, TAPS) and LBL (TPC), enable the investigation of the emission pattern and correlations of primary and secondary particles in a far more detailed manner than ever before. It is now for the first time possible to thoroughly investigate correlation phenomena such as in–plane bounce–off [24–27] and out–of–plane squeeze–out [28–30] of *pions*. The detailed investigation of these effects, including their possible origin and their impact parameter and p_t dependencies as well as their sensitivity to the nuclear equation of state, are the subject of this publication.

II. THE IQMD-MODEL

The first widely used microscopic models for the description of relativistic heavy ion collisions were based on the Vlasov–Uehling–Uhlenbeck (VUU) theory [18,31,32], which explicitly treats nonequilibrium and (stochastic) quantum effects in the framework of one–particle quantities, as well as the nuclear potential (nuclear equation of state). The dynamical basis of the VUU–model is the following transport equation:

$$\frac{\partial f}{\partial t} + \vec{v} \cdot \nabla_r f - \nabla_r U \cdot \nabla_p f \quad = \quad -\frac{4}{(2\pi)^3} \int \mathrm{d}^3 p_2 \, \mathrm{d}^3 p_1' \, \mathrm{d}\Omega \, v_{12} \frac{\mathrm{d}\sigma}{\mathrm{d}\Omega}$$

$$\times \, [f f_2 (1 - f_1')(1 - f_2') - f_1' f_2' (1 - f)(1 - f_2)]$$
$$\times \, \delta^3 (p + p_2 - p_1' - p_2').$$

f is the single–particle distribution function. The l.h.s. contains the potential U. Usually U is parameterized using the Skyrme ansatz. This gives the opportunity to study the effects of the nuclear equation of state via different parameter sets.

The r.h.s. contains the cross section σ and the Nordheim–Uehling–Uhlenbeck modifications incorporating the Pauli–blocking factors [33]. Models based on the same theory, but differing in numerical implementation, are the Boltzmann–Uehling-Uhlenbeck (BUU) [32] and the Landau–Vlasov [34] model. All 3D-numerical implementations of the VUU theory are solved with the test particle method. The number of test particles used to represent a nucleon varies with the numerical implementation. The test particle method solvs Hamilton's equation of motion for each test particle. These transport models have been successful in studying various aspects of relativistic heavy ion collisions, such as single particle spectra, collective effects (stopping, bounce–off, squeeze–out) and meson production.

However, certain fluctuations and correlations, such as the formation of fragments in relativistic heavy ion collisions, cannot be studied with a transport model based on a single–particle distribution function. This was one of the motivations for the developement of the **Q**uantum **M**olecular **D**ynamics model (QMD) [21,35–37]. In the QMD model the baryons are represented by Gaussian shaped density distributions

$$f_i(\vec{r}, \vec{p}, t) = \frac{1}{\pi^2 \hbar^2} e^{-(\vec{r} - \vec{r}_{i0}(t))^2 \frac{1}{2L}} e^{-(\vec{p} - \vec{p}_{i0}(t))^2 \frac{2L}{\hbar^2}}$$

They are initialized in a sphere of a radius $R = 1.14 A^{1/3}$ fm, in accord with the liquid drop model. Each nucleon occupies a volume of h^3, so that phasespace is uniformly filled. The initial momenta are randomly choosen between 0 and the local Thomas-Fermi-momentum. The A_P and A_T nucleons interact via two- and three- body skyrme forces, a Yukawa potential and momentum dependent interactions. Subsequently, the FMD [38], AMD [39] and PQMD [40] models have been developed to offer an improved treatment of the Pauli-principle.

Isospin is treated explicitely (in the socalled "I"QMD version), a symmetry potential (to achieve corrected distributions of protons and neutrons in the nucleus) and explicit Coulomb forces between the Z_P and Z_T protons are included.

Pion production is treated via the delta resonance [24,41,42]. A frozen Δ approximation (infinite lifetime for the Δ resonance) had been used in other versions of the QMD model.

The hadrons are propagating under the influence of the potential in Hamilton's equations of motion:

$$\dot{p}_i = -\frac{\partial H}{\partial q_i} \qquad \dot{q}_i = \frac{\partial H}{\partial p_i}$$

with

$$H = T + V = \sum_i \frac{p_i^2}{2m_i} + \sum_i \sum_{j>i} \int f_i(\vec{r}, \vec{p}, t) \, V^{ij} f_j(\vec{r}', \vec{p}', t) \, d\vec{r} \, d\vec{r}' d\vec{p} \, d\vec{p}' \quad .$$

The baryon-potential $V^{ij} = V_{loc}^{ij} + V_{Yuk}^{ij} + V_{Coul}^{ij} + V_{mdi}^{ij} + V_{sym}^{ij}$ consists of

$$V_{loc}^{ij} = t_1 \delta(\vec{r}_i - \vec{r}_j) + \sum_{k>j>i} \int f_k(\vec{r}'', \vec{p}'') t_2 \delta(\vec{r}_i - \vec{r}_j) \delta(\vec{r}_i - \vec{r}_k) d\vec{r}'' d\vec{p}''$$

$$V_{Yuk}^{ij} = t_3 \frac{\exp\{|\vec{r}_i - \vec{r}_j|/\mu\}}{|\vec{r}_i - \vec{r}_j|/\mu}$$

$$V_{Coul}^{ij} = \frac{Z_i Z_j e^2}{|\vec{r}_i - \vec{r}_j|}$$

$$V_{mdi}^{ij} = t_4 \ln^2(1 + t_5(\vec{p}_i - \vec{p}_j)^2)\delta(\vec{r}_i - \vec{r}_j)$$

$$V_{sym}^{ij} = t_6 \frac{1}{\varrho_0} T_{3i} T_{3j} \delta(\vec{r}_i - \vec{r}_j)$$

The three-body term in V_{loc}^{ij} as stated above is only valid for a hard equation of state (for a soft equation of state a VUU-type formulation $\sim \rho^\gamma$ has to be used), Z_i, Z_j denote the charges of the baryons i and j and T_{3i}, T_{3j} are their respective T_3 components. The meson-potential only consists of the Coulomb potential.

The parameters μ and $t_1 ... t_6$ are adjusted to the real part of the nucleon optical potential. For the density dependence of the nucleon optical potential standard Skyrme type parametrizations are used. Two different equations of state have been implemented: A hard equation of state (H) with a compressibility of 380 MeV and a soft equation of state (S) with a compressibility of 200 MeV [18,31]. A fit of the momentum dependence to measurements [43,44] of the real part of the nucleon optical potential [6,21,45] yields:

$$\delta \cdot \ln^2\left(\varepsilon \cdot (\Delta \vec{p})^2 + 1\right) \cdot \left(\frac{\rho}{\rho_0}\right)$$

The equation of state in its standard Skyrme type parametrization including momentum dependence then reads:

$$U = \alpha \cdot \left(\frac{\rho}{\rho_0}\right) + \beta \cdot \left(\frac{\rho}{\rho_0}\right)^\gamma + \delta \cdot \ln^2\left(\varepsilon \cdot (\Delta \vec{p})^2 + 1\right) \cdot \left(\frac{\rho}{\rho_0}\right)$$

The mean field notation with the parameters $\alpha, \beta, \gamma, \delta$ and ϵ has been chosen for reasons of simplicity and in order to compare the parameters with those used in VUU/BUU calculations. Their values can be found in table I. While the forces are calculated via the

nucleon density in VUU/BUU calculations, a sum over two-particle interactions is performed in QMD/IQMD calculations.

The parameters $t_1...t_6$ are calculated in the IQMD model before the initialization of the projectile and target nuclei from the tabulated values of $\alpha, \beta, \gamma, \delta$ and ϵ which serve as input. The width and normalization of the Gaussian wave-packets have to be taken into account for the proper determination of the force-parameters.

Hard N-N-collisions are included by employing the collision term of the well known VUU/BUU equation [4,18,32,46,47]. The collisions are done stochastically, in a similar way as in the cascade models [48,49]. Two particles collide if their minimum distance d fulfills

$$d \leq d_0 = \sqrt{\frac{\sigma_{\text{tot}}}{\pi}}, \qquad \sigma_{\text{tot}} = \sigma(\sqrt{s}, \text{ type}).$$

"type" denotes the ingoing collision partners ($N-N, N-\Delta, N-\pi...$). In addition, the Pauli blocking (of the final state) of baryons is taken into account by checking the phase space densities in the final states of a two body collision. The final phase space fractions P_1 and P_2 which are already occupied by other nucleons are determined for each of the two scattering baryons. The particular attempt for a collision is then blocked with the probability

$$P_{block} = 1 - (1 - P_1)(1 - P_2)$$

Whenever an attempted collision is blocked the scattering partners maintain the original momenta prior to scattering. Delta decays are checked in an analogous fashion with respect to the phase space of the resulting nucleon.

Pions are formed in the IQMD model via the decay of the delta resonance. The following inelastic reactions are explicitly taken into account and constitute the imaginary part of the pion optical potential, which is dominant in the 1 GeV/u energy domain [50]:

$$\begin{aligned}
\text{a)} \quad & N\,N \;\rightarrow\; \Delta\,N \quad (hard\text{--}delta\text{--production}) \\
\text{b)} \quad & \Delta \;\rightarrow\; N\,\pi \quad (\Delta\text{--decay}) \\
\text{c)} \quad & \Delta\,N \;\rightarrow\; N\,N \quad (\Delta\text{--absorption}) \\
\text{d)} \quad & N\,\pi \;\rightarrow\; \Delta \quad (soft\text{--}delta\text{--production})
\end{aligned}$$

Elastic $\pi-\pi, \pi-N, \pi-\Delta, \Delta-\Delta, \Delta-N$ scattering is not taken into account. Experimental cross sections are used for processes a) and d) [51], as well as for the elastic N-N-collisions. The respective cross sections are shown in figure 1.

For the delta absorption, process c), we use a modified detailed balance formula [52]. The conventional detailed balance formula is only correct for particles with infinite lifetimes (zero width). If the principle of detailed balance is applied to the delta resonance, then its finite width has to be taken into account:

$$\frac{d\sigma^{N\Delta \to NN}}{d\Omega} = \frac{1}{4} \frac{m_\Delta p_{NN}^2}{p_{N\Delta}} \frac{d\sigma^{NN \to N\Delta}}{d\Omega} \left(\frac{1}{2\pi} \int\limits_{m_N+m_\pi}^{\sqrt{s}-m_N} p_{N\Delta} A_r(M) 2M \, dM \right)^{-1}$$

with

$$A_r(M) = \frac{\Gamma/2}{(M - m_\Delta)^2 + (\Gamma/2)^2}$$

The mass-dependent Δ–decay width has been taken from [53]:

$$\Gamma_\Delta(p_\pi) = \frac{r(p_\pi)}{r(p_0)} \Gamma_0 \qquad \text{with} \quad r(p) = \frac{p^3}{1 + \left(\frac{p}{p_1}\right)^2 + \left(\frac{p}{p_1}\right)^4} \quad .$$

p_π is the decay momentum of the pion, $p_0 = 227$ MeV/c, $p_1 = 238$ MeV/c, $p_2 = 318$ MeV/c and $\Gamma_0 = 120$ MeV. The Δ decays isotropically in its restframe.

The elastic nucleon–nucleon scattering angular distribution is taken to be [54]:

$$\frac{d\sigma_{\text{el}}}{d\Omega} \sim \exp(A(s) \, t) \quad ,$$

where t is $-q^2$, the squared momentum transfer and

$$A(s) = 6 \frac{(3.65 \, (\sqrt{s} - 1.8766))^6}{1 + (3.65 \, (\sqrt{s} - 1.8766))^6} \quad .$$

$\sqrt{s}$ is the c.m. energy in GeV and A is given in $(\text{GeV/c})^{-2}$.

The inealstic channel is treated in an analogous fashion. The parametrization suggested by Huber and Aichelin [55] is used: fitted differential cross sections are extracted from OBE calculations:

$$\frac{d\sigma_{\text{in}}}{d\Omega} \sim a(s) \, \exp(b(s) \, \cos\theta) \quad ,$$

$a(s)$ and $b(s)$ are functions of $\sqrt{s}$ and vary in their definition for different intervals of $\sqrt{s}$ (see table II).

Pions propagate between collisions (imaginary part of the pion optical potential) on curved trajectories with Coulomb forces acting upon them. The different isospin channels are taken into account using the respective Clebsch–Gordan–coefficients:

$$\Delta^{++} \to 1(p + \pi^+) \qquad\qquad \Delta^+ \to \tfrac{2}{3}(p + \pi^0) + \tfrac{1}{3}(n + \pi^+)$$
$$\Delta^0 \to \tfrac{2}{3}(n + \pi^0) + \tfrac{1}{3}(p + \pi^-) \qquad \Delta^- \to 1(n + \pi^-)$$

The real part of the pion optical potential is treated in the following manner: As far as the pion is bound in a Δ-resonance, the density and momentum dependent real part of the

nucleon optical potential is applied as an approximation to the (yet unknown) real part of the Δ optical potential. Due to the large $\pi - N$ cross section, intermediate pions are quite frequently bound in a Delta resonance and in that intervals the real part of the pion optical potential is substituted by the real part of the Δ optical potential. Free intermediate and final charged pions experience coulomb forces which contribute to the real part of the pion optical potential. Recent investigations on the influence of the nuclear medium correction to the dispersion relation of the free pion have shown conflicting results [56,57] with respect to the importance of the modification for low momentum pions. However, both calculations show that the high energy part of the pion spectrum remains unchanged by this modification. Since our results are mainly for this high energy contribution we omit this medium correction, until a consensus has been achieved on the proper form of the respective medium contribution.

After a pion is produced (be it free or *bound* in a delta), it's fate is governed by two distinct processes:

1. absorption $\pi\,N\,N \to \Delta\,N \to N\,N$

2. scattering (resorption) $\pi\,N \to \Delta \to \pi\,N$

In the CASCADE mode all real forces are turned off: nucleons, pions and deltas are propagated on straight lines between collisions.

III. FORMATION AND SPECTROSCOPY OF Δ RESONANCE MATTER

Recently an old subtopic [10,58] of this research has received renewed attention [59–63]: The possibility of producing Δ-*matter* (or in more general terms: *resonance matter*). At beam energies above a few hundred MeV/nucleon, the nucleons can be excited into Δ-resonances. If the density of these resonances is as high as the nuclear matter ground state density, then a new state of matter, Δ-*matter*, has been created. One of the potential signals for the presence of Δ-*matter* is the creation of pions as decay-products of the Δ-resonance.

How can Δ-*matter* be produced? Figure 2 shows the pion – nucleon cycle in the IQMD model. The scheme describes (for impact parameters b $\leq$ 5 fm and averaged over 60 fm/c possible processes linked to the creation of Δ-*matter*. The probabilities in the boxes always refer to the vertices they are directly connected with. Δ-resonances are initially produced via inelastic nucleon nucleon scattering. The produced resonances can either be reabsorbed via inelastic scattering or decay by emitting a pion. The pion can then either *freeze out* or interact with a nucleon to form a Δ again. In case the Δ has been absorbed the corresponding

high energetic ergetic nucleon might have a second chance of becoming a Δ by inelastic scattering. It could also transfer energy via elastic scattering onto another nucleon which then could scatter inelastically and form a new Δ. A nucleon interacts in the average about three times before it freezes out. This value fluctuates considerably, depending on whether the nucleon was in the participant zone (geometrical overlap of the colliding heavy ions) or in the spectator zone of the collision.

Unfortunately, the probablity for a nucleon to undergo inelastic scattering and to form a Δ during the heavy ion collision is as low as 10%. The main process for sustaining Δ-*matter* is the $\Delta \to N\pi \to \Delta$ loop, which, however, first has to be fueled by the $NN \to \Delta N$ process. The average pion passes approximately three times through this loop (it has been created by the decay of a *hard* Δ). However, 30% pass more than 6 times through the loop. For nucleons the probability of forming a *soft* Δ i.e. via $\pi N \to \Delta$ is almost twice as high (Δ-*matter pump*) than the probability of forming a *hard* Δ via $NN \to N\Delta$.

Figure 3a) shows the time evolution of the total baryon, nucleon and Δ densities in units of ρ/ρ_0 (top). The densities are calculated in a sphere of 2 fm radius around the collision center. Between 5 fm/c and 20 fm/c more than 20 Δ-resonances can be found in the system: This time interval coincides with the hot and dense reaction phase. At 10 fm/c up to 55 resonances are present in the *total* reaction volume (keep in mind this is *not* in the 2 fm test sphere). A Δ multiplicity of > 40 can be sustained for an interval of 10 fm/c, 6 times longer than the lifetime of a free Δ-resonance. However, this is not pure Δ-*matter*: in the small *test* volume shown in figure 2a the resonance *density* is 0.5 ρ_0 and the nucleon density is 2.2 ρ_0: the Δ-contribution is 20% in the test volume which contains, as a matter of fact, only 2.5 resonances. The total multiplicity of Δ resonances is just about 10% of the total nucleon multiplicity.

However, it is obvious that the other Δs can be distributed all over the reaction volume. Figure 3b) shows the Δ density distribution as experienced by the Δ's in the system at 5, 10 and 20 fm/c. The densities were calculated by summing over all contributing Gaussians of all Δs in the system at the locations of the respective Δs. We would like to point out that the mean Δ-density experienced by the Δs is about 0.25 ρ_0. Less than 1% of the Δs experience Δ densities around 0.5 ρ_0. However, enough Δs are in the system to show signs of collectivity such as *collective flow* in the reaction plane. Its measurable signiture (the pion $\vec{p}_x(y)$ distribution in central collisions) will be discussed in one of the follwing sections.

IV. INCLUSIVE PION OBSERVABLES

This section deals with inclusive pion production in relativistic heavy ion collisions. Figure 4 shows the predicted impact parameter dependence of the multiplicity of π^-, π^0 and π^+ for Au+Au collisions at 1 GeV/nucl. incident beam energy. A hard EoS with momentum dependent interaction is used in the calculation. For central collisions ($b = 0$ fm) the total pion multiplicity is approximately 55. However, the average pion multiplicity is about 19 (8 π^-, 6 π^0 and 5 π^+) for a minimum bias impact parameter distribution.

The mass dependence of the total pion multiplicity is shown in figure 5. For light collision systems the multiplicity increases linearly with the system mass. However, for heavier systems the increase is less than the linear extrapolation, this is due to pion absorption. The values are for $b = 0$ fm calculations of the systems ^{20}Ne+^{20}Ne, ^{40}Ca+^{40}Ca, ^{58}Ni+^{58}Ni, ^{93}Nb+^{93}Nb and ^{197}Au+^{197}Au.

The polar angular distribution $\frac{dN}{d\cos\vartheta_{c.m.}}$ for π^-, π^0 and π^+ is shown in Figure 6 for minimum bias events (a) and for π^- in central vs. minimum bias events in (b). A horizontally flat distribution would correspond to isotropic emission. For minimum bias events (top) a strong peaking towards forward–backward angles is observed, most prominently for π^-.

This is important for the extrapolation of total yields from spectra measured at $\vartheta_{c.m.} = 90°$ – if the midrapidity spectra are used to extrapolate (with the assumption of a flat distribution) the total yield may be underestimated by a factor of 2. The anisotropy decreases when studying central collisions (bottom). This dependence can be explained by the decay of Δ-resonances in the projectile- and target- spectator regions. The difference betweeen the distributions of π^- and π^+ also results in a forward–backward peaking of the N_{π^-}/N_{π^+} ratio. This phenomenon has already been experimentally observed for light collision systems at the BEVALAC [64].

Figure 7 shows a comparison of inclusive π^0 spectra for Au+Au and Ca+Ca (minimum bias and $y_{c.m.} \pm 0.16$) between the IQMD model and data published by the TAPS collaboration [65]. Whereas the model shows reasonable agreement with the heavy system Au+Au it overpredicts the π^0 yield of the light system Ca+Ca by approximately 60%. The charged pions (for Au+Au collisions) are shown in figure 8 together with π^+ data from the KaoS collaboration [66]. The slope of the π^+ spectrum in the model calculation agrees well with the KaoS measurements. However, the multiplicity as predicted by the model is approximately 20% above the KaoS measurements. Both, the calculation and the measurements, have been acceptance corrected to the rapidity interval $y_{c.m.} \pm 0.16$ and may directly be compared to Figure 7. Especially the measurement of high energy pions is of great interest.

They correlate directly to early freeze out times and heavy Δ resonances [67].

The mass dependence of pion production and its sensitivity towards the transverse momentum p_t can be studied more clearly by plotting the ratio of the p_t spectra for Au+Au and Ca+Ca versus the transverse momentum p_t (Figure 9). A comparison between data from the TAPS collaboration [65] and the IQMD model is shown in figure 9. The model underpredicts this ratio by approximately a factor of 2, In particular for low transverse momenta . However, this holds for all transport model calculations which have been compared to the TAPS data [65]. A previous comparison between the IQMD model and the TAPS data in ref. [65] showed far larger disagreement between model and data. This was due to an improper normalization of the theoretical calculations.

The yield of low p_t pions in the heavy system is underpredicted by 10%. This is a common problem of most transport theories dealing with heavy ion collisions. Suggested explanations for this underprediction include in-medium effects of pions in nuclear matter [57] and the neglect of Bose-enhancement due to the bosonic nature of the pions.

The importance of the inclusion of Coulomb forces and energy dependent $\pi - N$ cross sections can be shown by plotting the π^- to π^+ ratio versus the transverse momentum p_t (Figure 10). The solid line shows the full calculation including Coulomb forces. For high p_t the π^-/π^+ ratio decreases towards 1, whereas for low p_t it increases to 2.5 – considerably higher than the value of 1.8 predicted by the Δ-isobar model. The dashed line shows a calculation without Coulomb forces. This ratio remains constant at 1.8. The (small) remaining variations might be due to the different energy dependence of the $\pi^+ - p$ and $\pi^- - p$ inelastic cross sections.

V. PION NUCLEON CORRELATION IN THE EVENT-PLANE

The hydrodynamical model predicts a bounce–off of nuclear matter in the reaction plane [8,68] which has experimentally indeed been discovered [69,70]. The bounce–off is depicted by plotting the in–plane transverse momentum $\vec{p_x}(y)$ versus the rapidity y. For nucleons and light fragments a horizontal s–shape is typically seen with negative $\vec{p_x}(y)$ values for $y \leq y_{c.m.}$ and positive $\vec{p_x}(y)$ values for $y \geq y_{c.m.}$. Figure 11 shows the $\vec{p_x}(y)$ distribution for π^+ and protons in Au(1AGeV)Au collisions with a minimum bias impact parameter distribution. The protons show the expected collective flow [71–73]. The $\vec{p_x}$ of the pions, however, is anticorrelated to that of the protons. A similar proton $-\pi$ anticcorrelation has been measured for the asymmetric system Ne+Pb at 800 MeV/nucl. by the DIOGENE collaboration [74]. Transport model comparisons to the DIOGENE data with the IQMD

10

[24] and the BUU [25] model have shown good agreement with the data.

We have studied the origin of the particular shape of the pion angular distribution and the $\vec{p_x}$ spectrum by sequentially suppressing first the *soft-delta*-production and then the delta-absorption (while allowing the *soft-delta*-production). If we deactivate the *soft–delta–production* (see Figure 3), $\pi N \rightarrow \Delta$, pions are neither scattered nor absorbed after the initial production. No $\vec{p_x}$ for pions is observed. In order to decide whether the $\vec{p_x}$ spectrum is caused by absorption or by scattering we now deactivate the reaction $\Delta N \rightarrow N N$. We thus suppress pion absorption but allow scattering – the anticorrelation between pions and protons in the $\vec{p_x}$ returns. In contrast to previous publications, which investigated the asymmetric system Ne(800AMeV)Pb and suggested the anticorrelation of pionic and nucleonic $\vec{p_x}$ at target rapidities to be caused by pion absorption [25], our investigation reveals the $\vec{p_x}$ spectrum of the pions to be dominated by the pion scattering process [26].

The following simplified picture can explain the origin of the observed phase space distribution: The Δ decays isotropically in its rest–frame, therefore 50 % of the pions are emitted with a positive p_x and 50 % with a negative p_x. At target rapidity those pions which obtain a positive p_x–value usually do not have the chance to rescatter: Most of the target nucleons are located in the *negative p_x area!* Those pions which *do* rescatter at target rapidity are the ones with an initially *negative p_x*: Every time a Δ decays (isotropically) there is a 50% chance that this pion is emitted *upward*, i.e. into an azimuthal angle between $-90° \leq \phi \leq 90°$. These ϕ–values characterize the hemisphere of positive p_x, by definition. This leads for $\approx$ 50% of the pions with – originally – negative p_x to a shift towards a positive p_x. This remains true even after transforming back into the laboratory frame. The same consideration applies vice versa for projectile rapidity: Most projectile nucleons are located in the *positive p_x area*. The pions are rescattered in this area which results in a negative $\vec{p_x}$ and a maximum in the azimuthal angular distribution in the $90° \leq \phi \leq 270°$ interval.

Figure 12 shows the in–plane transverse momentum $\vec{p_x}$ versus rapidity y (in the c.m. system) for π^+ in central collisions of Au+Au (with impact parameters b$\leq$ 3 fm). In contrast to (semi-) peripheral collisions, however, $\vec{p_x}$ is correlated for pions and nucleons in central collisions because of the bounce–off of Δ-resonances [75]. The square markers in Figure 12 depict a calculation with the hard equation of state without momentum dependence, the circles show the same equation of state including momentum dependence whereas the triangles represent a CASCADE calculation, i.e. a non-equilibrium free gas.

The momentum dependence enhances the $\vec{p_x}$ of the pions. This effect is due to the bounce–off of the Δ resonances [75] which in our model is enhanced because the momentum dependence for the Δ resonances is included in the same way as for the nucleons.

The CASCADE calculation, however, shows the opposite behaviour. The $\vec{p_x}$ of the pions has negative sign to that of the calculations with the density dependent equations of state. This behaviour can be explained by the lack of hadron collective flow in CASCADE calculations [76]. The pions would then be expected to be emitted isotropically ($\vec{p_x}(Y) = 0$). However, pion scattering from small caps of spectator matter being present at impact parameters around 3 fm causes the observed anticorrelation [26]. In order to investigate the density dependence of the nuclear equation of state and in order to show the differences between CASCADE calculations and calculations including the equation of state more clearly we use the robust observable p_x^{dir} which for nucleons is defined as

$$
p_x^{dir} = \frac{\sum\limits_{i=1}^{A_P+A_T} p_x^i \cdot \text{sgn}(y_i - y_{c.m.})}{A_T + A_P} \quad .
$$

(the adaptation for pions is straightforward) and plot it versus the impact parameter (Figure 13). For positive values of p_x^{dir} the pion $\vec{p_x}$ vs. rapidity distribution is correlated to that of the nucleons. For negative values an anticorrelation is observed.

Figure 13 shows the respective calculations for the hard and soft equations of state (including momentum dependence) and for the CASCADE calculation. For small impact parameters the calculations with equation of state show a correlation between pion and nucleon bounce–off. At semiperipheral impact parameters we observe a sign reversal. As mentioned above, the anticorrelation between nucleon and pion bounce–off is caused by pion scattering in spectator matter [26]. In contrast, the CASCADE calculation exhibits a negative p_x^{dir} for the whole impact parameter range. The momentum transfer p_x^{dir} shows a systematic difference between the hard and soft equation of state. However, very high statistics and high precision impact parameter classification are necessary to experimentally exploit this sensitivity towards the determination of the nuclear equation of state. The results of figures 11 and 13 show clearly that even in the domain of particle production ($\pi, K, \eta, \bar{p}, \rho, \omega$) CASCADE simulations predict distinctly different phase space distributions for baryons and mesons at central impact parameters.

VI. AZIMUTHAL CORRELATIONS OF PIONS PEPENDICULAR TO THE EVENT PLANE

Now let us investigate particle emission perpendicular to the reaction plane. The hydrodynamical model predicted a squeeze–out of high energetic nucleons perpendicular to the reaction plane [9,4,77]. This effect, which has also been predicted by QMD–calculations

[24,78–81] and has been confirmed by experiment [82–84], is due to the high compression of nuclear matter in the central hot and dense reaction zone (it is a genuinly collective effect, increasing linearly with A).

Do pions show a similar behaviour? The azimuthal (φ) distribution of the pions is plotted to investigate this question. φ is the angle between the transverse momentum vector $\vec{p_t}$ and the x-axis (which lies in the reaction plane and is perpendicular to the beam axis). Thus $\varphi = 0°$ denotes the projectile hemisphere and $\varphi = 180°$ corresponds to the target hemisphere.

Figure 14 shows the respective distributions for neutral pions in the transverse momentum bins $p_t \leq 50$ MeV and $p_t \geq 400$ MeV at a minimum bias impact parameter distribution. The distributions have been normalized in order to fit into the same figure. The analysis was performed from 0° to 180° and then symmetrized for 180° to 360°. The plotted distributions have been extracted by fitting the calculated points (shown for the high p_t bin) according to the function $a \cdot (1 + b \cdot \cos(\phi) + c \cdot \cos(2\phi))$. The azimuthal angular distribution for π^0 with low p_t shows maxima at $\varphi = 0°$ and $\varphi = 180°$ corresponding to a preferential emission in the reaction plane. The high p_t π^0, however, show a maximum at $\varphi = 90°$. This maximum is associated with preferential particle emission perpendicular to the reaction plane. The inlay shows data from the TAPS collaboration [30] for the region 400 MeV $\leq p_t \leq$ 600 MeV and midrapidity. We observe a good qualitative agreement between the theoretical prediction and the experiment. It should be noted, however, that both, theory and experiment, need much better statistics to allow a conclusive quantitative comparison.

The magnitude of the observed anisotropy and its dependence on impact parameter and transverse momentum is best studied by using the following ratio:

$$R_{out/in} = \left. \frac{\frac{dN}{d\varphi}(\varphi = 90°) + \frac{dN}{d\varphi}(\varphi = 270°)}{\frac{dN}{d\varphi}(\varphi = 0°) + \frac{dN}{d\varphi}(\varphi = 180°)} \right|_{y=y_{c.m.}}$$

For positive $R_{out/in}$ values pions are emitted preferentially perpendicular to the reaction plane. Figure 15 shows the transverse momentum dependence of $R_{out/in}$ for Au+Au collisions with an impact parameters bewteen b=5 fm and b=10 fm and at midrapidity ($y_{c.m.} = \pm 0.2$): In contrast to pions with low transverse momentum, which are emitted preferentially in the reaction plane, high p_t pions are preferentially emitted perpendicular to the reaction plane. This effect is stronger for π^+ than for π^-. The difference is due to the different $\pi N \rightarrow \Delta$ production cross section for π^+ and π^- and due to Coulomb forces pushing the π^+ away from the spectator matter which is located mostly in the reaction plane. The π^- on the other hand are being attracted by those spectator-protons. These effects decrease the number of π^- leaving the reaction zone in a direction perpendicular to the reaction-plane.

However, the statistics accumulated so far are not large enough for a more detailed study of the differences between positive and negative pions. The inlay of Figure 15 shows recent measurements from the KaoS collaboration [29] which confirm the predicted systematics of the p_t dependence. Imposing the limited acceptance of the KaoS spectrometer on the IQMD calculations would reduce the available statistics by one order of magnitude. Experimental uncertainties in the determination of the proper reaction plane result in a reduction of the measured $R_{out/in}$ values which are difficult to compensate. Therefore a direct quantitative comparison between the KaoS measurements and IQMD calculations is not feasable at this point of time.

We have investigated the cause of the observed preferential emission perpendicular to the reaction plane: Pion absorption as well as scattering can be eliminated by deactivating the reaction $\pi N \to \Delta$, then no sqeeze-out is observed.

In order to decide whether the anisotropy is caused by absorption or by scattering the reaction $\Delta N \to N N$ can be deactivated. Thus pion absorption is suppressed but scattering is allowed: no anisotropy is observed. Therefore we conclude that the anisotropy is dominated by the pion absorption process [28].

Figure 16 shows the distribution of the number of delta generations n_Δ a pion goes through before its freeze out. Here n_Δ is shown for π^+ emitted both in the reaction plane as well as perpendicular to it. $(n_\Delta - 1)$ is therefore the number of times a pion scatters before freeze out. We observe that 90% of the produced pions scatter at least once before leaving the reaction zone. A large number of pions scatters even more often, 2% up to 10 times! The observed preferential emission perpendicular to the reaction plane is due to an excess of high p_t pions which on the average have undergone fewer collisions (≤ 2) than the pions in plane. Those pions which make this effect do rescatter rarely, they are emitted early but carry information on the high density phase of the reaction. They stem from the decay of the most massive delta resonances which are mostly produced early on in the reaction [67]. Therefore high p_t pions emitted perpendicular to the event-plane should be the most sensitive pionic probes for the investigation of the hot and early reaction zone.

Figure 17 shows the azimuthal angular distribution of high p_t ($p_t \geq 400$ MeV) neutral pions at midrapidity and impact parameter b=6 fm. The different curves show calculations for hard (circles) and soft (squares) equations of state (including momentum dependence) and a CASCADE calculation (triangles). φ is the angle between the transverse momentum vector $\vec{p_t}$ and the x-axis (which lies in the reaction plane and is perpendicular to the beam axis). The out–of–plane pion squeeze–out is clearly seen by the pronounced maximum at $\varphi = 90°$ for both equations of state. To enhance the statistics all particles are projected

into the $0° \leq \varphi \leq 180°$ hemisphere. The full and dashed lines are least square fits with the function $f(\varphi) = a(1 + s_1 \cos(\varphi) + s_2 \cos(2\varphi))$ which has been used to fit the squeeze–out phenomenon [82,83]. The curves show an extrapolation to the full azimuthal angular range. The distributions are normalized per particle in order subtract the influence of different equations of state on the pion multiplicity. Within error-bars both equations of state exhibit the same out–of–plane pion squeeze–out. There is a trend for the hard equation of state to exhibit an enhanced out–of–plane pion squeeze–out but this trend might be too small to be useful for an experimental distinction between the different equations of state, whereas – in contrast – the in–plane pion bounce–off shows a clear difference for the two cases (see above). The CASCADE calculation does not exhibit any significant out–of–plane pion squeeze–out for b=6 fm! However, for larger impact parameters also CASCADE calculations exhibits a pronounced out–of–plane pion squeeze–out (Figure 18).

Figure 18 shows $R_{out/in}$ versus impact parameter b for the hard equation of state with and without momentum dependence of the real part of the nucleon optical potential. The momentum dependence causes a drastic increase of $R_{out/in}$ for impact parameters larger than 3 fm. In the CASCADE calculation the onset of the out–of–plane pion squeeze–out is shifted toward larger impact parameters as compared to the calculations including the equation of state (see also Figure 17). For peripheral collisions $R_{out/in}$ reaches the same magnitude for the CASCADE calculation and the hard equation of state without momentum dependence.

VII. CONCLUSION AND OUTLOOK

The physics responsible for the in–plane *pion* bounce–off (pion scattering) and the out–of–plane *pion* squeeze–out (pion absorpion) differs completely from the compressional effects governing the in–plane *nucleon* bounce–off and out–of–plane *nucleon* squeeze–out. It is the pion–nucleon interaction which creates the sensitivity towards the density and momentum dependence of the nucleon optical potential. Therefore it is understandable that we observe a strong sensitivity towards the equation of state *in* the reaction plane whereas the sensitivity towards the equation of state *perpendicular* to the reaction plane is limited to the momentum dependence: The (anti-) correlation in–plane is caused by multiple pion nucleon scattering [26] with the bounced–off nucleons, which show a strong sensitvity towards momentum and density dependence [41]. The pion squeeze–out perpendicular to the reaction plane, however, is dominated by high p_t pions which have undergone less rescattering than those in the reaction plane [28]. The abundance of these high p_t pions is correlated to the multiplicity of high p_t nucleons which increases if the density dependence is included.

We have investigated the dependence of *pionic* in–plane bounce–off and out–of–plane squeeze–out on the *nuclear* equation of state. A strong sensitivity towards the *density dependence* is observed for the in–plane *pion* bounce–off whereas the out–of–plane *pion* squeeze–out shows only a small sensitivity. Both effects show a strong sensitivity toward the *momentum dependence.* CASCADE caluculations – which we see as a crude approximation to QMD – give different phase space distributions for pions in both cases. It should be easy to resolve experimentally these two clearly qualitatively different distinct scenarios. The determination of the equation of state will require – on the other hand – a more sensitive (and sensible) quantitative comparison to theory, including a improved treatment of the Δ and pion optical potential.

The nuclear equation of state cannot be extracted from one observable alone. All observables known to be sensitive to the equation of state have to be fitted simultaneously by the respective model in order to claim success. In this article we have added additional, here *pionic*, observables which have to be taken into account for obtaining the final goal: The nuclear equation of state.

REFERENCES

[1] W. Scheid, R. Ligensa, and W. Greiner. Phys. Rev. Lett. **21**, 1479 (1968).

[2] L. P. Csernai and J. I. Kapusta. Phys. Reports **131**, 225 (1986).

[3] R. Stock. Phys. Reports **135**, 261 (1986).

[4] H. Stöcker and W. Greiner. Phys. Reports **137**, 277 (1986).

[5] R. B. Clare and D. Strottman. Phys. Reports **141**, 179 (1986).

[6] B. Schürmann, W. Zwermann and R. Malfliet. Phys. Reports **147**, 3 (1986).

[7] W. Cassing, V. Metag, U. Mosel and K. Niita. Phys. Reports **188**, 365 (1986).

[8] H. Stöcker, J. A. Maruhn and W. Greiner, Phys. Rev Lett. **44**, 725 (1980).

[9] H. Stöcker, L. P. Csernai, G. Graebner, G. Buchwald, H. Kruse, R. Y. Cusson, J. A. Maruhn and W. Greiner, Phys. Rev **C25**, 1873 (1982).

[10] H. Stöcker, W. Greiner, and W. Scheid. Z. Phys. **A286**, 121 (1978).

[11] P. Danielewicz. Nucl. Phys. **A314**, 465 (1979).

[12] H. Stöcker, A. A. Ogloblin and W. Greiner. Z. Phys. **A303**, 259 (1981).

[13] A. Sandoval, R. Stock, H. E. Stelzer, R. E. Renfordt, J. W. Harris, J. P. Brannigian, J. V. Geaga, L. J. Rosenberg, L. S. Schroeder and K. L. Wolf. Phys. Rev. Lett. **45**,874 (1980).

[14] R. Stock, R. Bock, R. Brockmann, J.W. Harris, A. Sandoval, H. Ströbele, K.L. Wolf, H.G. Pugh, L.S. Schroeder, M. Maier, R.E. Renfordt, A. Dacal and M.E. Ortiz. Phys. Rev. Lett. **49**, 1236 (1982).

[15] J. Harris, R. Bock, R. Brockmann, A. Sandoval, R. Stock, H. Stroebele, G. Odyniec, L. Schroeder, R. E. Renfordt, D. Schall, D. Bangert, W. Rauch, and K. L. Wolf. Phys. Lett. **B153**, 377 (1985).

[16] S. Nagamiya, M.C. Lemaire, E. Moeller, S. Schnetzer, G. Shapiro, H. Steiner, and I. Tanihata. Phys. Rev. **C24**, 971 (1981).

[17] G.F. Bertsch, H. Kruse and S. Das Gupta. Phys. Rev. **C29**, R673 (1984).

[18] H. Kruse, B. V. Jacak, and H. Stöcker. Phys. Rev. Lett. **54**, 289 (1985).

[19] A. Shor et al. Phys. Rev. Lett. **48**, 1597 (1982).

[20] J. Aichelin and C. M. Ko. Phys. Rev. Lett. **55**, 2661 (1985).

[21] J. Aichelin, A. Rosenhauer, G. Peilert, H. Stöcker, and W. Greiner. Phys. Rev. Lett. **58**, 1926 (1987).

[22] F. D. Berg and the TAPS collaboration. Phys. Rev. Lett. **72**, 977 (1994).

[23] D. Miskowiec and the KaoS collaboration. Phys. Rev. Lett. **72**, 3650 (1994).

[24] Ch. Hartnack, H. Stöcker, and W. Greiner. In H. Feldmeier, editor, *Proc. of the International Workshop on Gross Properties of Nuclei and Nuclear Excitation, XVI, Hirschegg, Kleinwalsertal, Austria* (1988).

[25] B. A. Li, W. Bauer, and G. F. Bertsch. **Phys. Rev. C** 44, 2095 (1991).

[26] S. A. Bass, C. Hartnack, R. Mattiello, H. Stöcker and W. Greiner. Phys. Lett. **B302**, 381 (1993).

[27] M. Trzaska and the FOPI collaboration. Proc. of the XXXII Winter Meeting on Nucl. Physics, Bormio, Italy, Jan. 1994.

[28] S. A. Bass, C. Hartnack, H. Stöcker and W. Greiner. Phys. Rev. Lett. **71**, 1144 (1993).

[29] D. Brill and the KaoS collaboration. Phys. Rev. Lett. **71**, 336 (1993).

[30] L. Venema and the TAPS collaboration. Pys. Rev. Lett. **71**, 835 (1993).

[31] J. J Molitoris and H. Stöcker, Phys. Rev **C32**, R346 (1985).

[32] J. Aichelin and G. Bertsch. Phys. Rev. **C31**, 1730 (1985).

[33] E. A. Uehling and G. E. Uhlenbeck. Phys. Rev. **43**, 552 (1933) and Phys. Rev. **44**, 917 (1934).

[34] C. Gregoire, B. Remaud, F. Sebille, L. Vinet, and Y. Raffray, Nucl. Phys. **A465**, 317 (1987).

[35] J. Aichelin and H. Stöcker. Phys. Lett. **B176**, 14 (1986).

[36] G. Peilert, H. Stöcker, A. Rosenhauer, A. Bohnet, J. Aichelin and W. Greiner. Phys. Rev. **C39**, 1402 (1989).

[37] J. Aichelin. Phys. Reports **202**, 233 (1991).

[38] H. Feldmeier. Nucl. Phys. **A515**, 147 (1990).

[39] A. Ono, H. Horiuchi, T. Maruyama and A. Ohnishi. Phys. Rev. Lett. **68**, 2898 (1992).

[40] G. Peilert, J. Konopka, M. Blann, M. G. Mustafa, H. Stöcker and W. Greiner. Phys. Rev. **C46**, 1457 (1992).

[41] C. Hartnack, L. Zhuxia, L. Neise, G. Peilert, A. Rosenhauer, H. Sorge, J. Aichelin, H. Stöcker, and W. Greiner. Nucl. Phys. **A495**, 303 (1989).

[42] Ch. Hartnack. PhD thesis, GSI-Report 93-5 (1993).

[43] L. G. Arnold et al. Phys. Rev. **C25**, 936 (1982).

[44] G. Passatore. Nucl. Phys. **A95**, 694 (1967).

[45] G. F. Bertsch and S. Das Gupta, Phys. Rep. **160**, 189 (1988).

[46] G. Wolf, G. Batko, W. Cassing, U. Mosel, K. Niita, and M. Schäfer. Nucl. Phys. **A517**, 615 (1990).

[47] B. A. Li and W. Bauer. Phys. Lett. **B252**, 335 (1991).
B. A. Li, W. Bauer, and G. F. Bertsch. Phys. Rev. **C44**, 450 (1991).

[48] Y. Yariv and Z. Frankel. Phys. Rev. **C20**, 2227 (1979).

[49] J. Cugnon. Phys. Rev. **C22**, 1885 (1980).

[50] A. Engel, W. Cassing, U. Mosel, M. Schäfer and Gy. Wolf. Nucl. Phys. **A572**, 657 (1994).

[51] B. J. VerWest and R. A. Arndt. Phys. Rev. **C25**, 1979 (1982).

[52] P. Danielewicz and G. F. Bertsch. Nucl. Phys. **A533**, 712 (1991).

[53] J. Randrup. Nucl. Phys. **A314**, 429 (1979).

[54] J. Cugnon, T. Mizutani and J. Vandermeulen. Nucl. Phys. **A352**, 505 (1981).

[55] S. Huber and J. Aichelin. Nucl. Phys. **A573**, 587 (1994).

[56] W. Ehehalt, W. Cassing, A. Engel, U. Mosel and Gy. Wolf. Phys. Lett. **B298**, 31 (1993).

[57] L. Xiong, C. M. Ko and V. Koch. Phys. Rev. **C47**, 788 (1993).

[58] G. F. Chapline, M. H. Johnson, E. Teller and M. S. Weiss. Phys. Rev. **D8**, 4302 (1973)

[59] J. Boguta. Phys. Lett **B109**, 251 (1982).
J. Boguta and H. Stöcker. Phys. Lett **B120**, 289 (1983).

[60] B. Waldhauser, J.A. Maruhn, H. Stöcker and W. Greiner. Z. Phys. **A328**, 19 (1987).

[61] V. Metag. Prog. Part. Nucl. Phys. **30**, 75 (1993).

[62] W. Ehehalt, W. Cassing, A. Engel, U. Mosel and G. Wolf. Pys. Rev. **C47**, R2467 (1993).

[63] M. Hofmann, R. Mattiello, N. S. Amelin, M. Berenguer, A. Dumitru, A. Jahns, A. v. Keitz, Y. Pürsün, T. Schönfeld, C. Spieles, L. A. Winckelmann, H. Sorge, J. A. Maruhn, H. Stöcker and W. Greiner. Nucl. Phys. **A566**, 15c (1994).

[64] W. Benenson et al.. Phys. Rev. Lett. **43**, 683 (1979).

[65] O. Schwalb and the TAPS collaboration. Phys. Lett. **B321**, 20 (1994).

[66] Ch. Müntz and the KaoS collaboration. Z. Phys. **A** in print.

[67] S. A. Bass, C. Hartnack, H. Stöcker and W. Greiner. Phys. Rev. **C50**, 2167 (1994).

[68] H. Stöcker, J. A. Maruhn and W. Greiner. Z. Phys. **A293**, 173 (1979).

[69] L. P. Csernai, W. Greiner, H. Stöcker, I. Tanihata, S. Nagamiya and J. Knoll. Phys. Rev **C25**, 2482 (1982).

[70] H. H. Gutbrod, A. M. Poskanzer and H. G. Ritter. Rep. Prog. Phys. **52**, 1267 (1989).

[71] J. J. Molitoris and H. Stöcker, Phys. Lett. **B162**, 47 (1985).

[72] H.-A. Gustafsson, H. H. Gutbrod, B. Kolb, H. Löhner, B. Ludewigt, A. M. Poskanzer, T. Renner, H. Riedesel, H. G. Ritter, A. Warwick, F. Weik, and H. Wieman. Phys. Rev. Lett. **52**, 1590 (1984).

[73] J. J. Molitoris, H. Stöcker, and B. L. Winer. Phys. Rev. **C36**, 220 (1986).

[74] J. Gosset O. Vallette, J. P. Alard, J. Augerat, R. Babinet, N. Basid, F. Brochard, N. De Marco, P. Dupieux, Z. Fodor, L. Faysse, P. Gorodetzky, M. C. Lemaire, D. L'Hote, B. Lucas, J. Marroncle, G. Montarou, M. J. Parizet, J. Poitou, C. Racca, A. Rahmani, W. Schimmerling and Y. Terrien. Phys. Rev. Lett. **62**, 1251 (1989).
J. Poitou and the DIOGENE collaboration. *Proceedings of the International Workshop on Gross Properties of Nuclei and Nuclear Excitations* XVI, Hirschegg, Kleinwalsertal, Austria, 1989.

[75] S. A. Bass, M. Hofmann, C. Hartnack, H. Stöcker and W. Greiner. Phys. Lett. **B335** (1994) 289.

[76] J. J. Molitoris, H. Stöcker, H. A. Gustafsson, J. Cugnon and D. L'Hôte. Phys. Rev. **C33**, 867 (1986).

[77] G. Buchwald, G. Gräbner, J. Theis, H. Stöcker, K. Frankel, M. Gyulassy, J. Maruhn and W. Greiner. Phys. Rev. **C28**, 2349 (1983).

[78] Ch. Hartnack, H. Stöcker and W. Greiner. Proc. of the Nato Adv. Study Inst. on the Nucl. Equation of State (Peñiscola, Spain), Editors W. Greiner and H. Stöcker, Plenum Press (1990).

[79] Ch. Hartnack, M. Berenguer, A. Jahns, A .v. Keitz, R. Mattiello, A. Rosenhauer, J. Schaffner, Th. Schönfeld, H. Sorge, L. Winckelmann, H. Stöcker and W. Greiner. Nucl. Phys. **A538**, 53c (1992).

[80] Ch. Hartnack, J. Aichelin, H. Stöcker and W. Greiner. Mod. Phys. Lett. in print.

[81] S. A. Bass, C. Hartnack, H. Stöcker and W. Greiner. GSI-preprint 94-12, submitted Z. Phys. **A**.

[82] H. H. Gutbrod, K. H. Kampert, B. W. Kolb, A. M. Poskanzer, H. G. Ritter, and H. R. Schmidt, Phys. Lett. **B216**, 267 (1989).

[83] H. H. Gutbrod, A. M. Poskanzer and H. G. Ritter. Rep. Prog. Phys. **52**, 1267 (1989).

[84] The LAND collaboration, Y. Leifels et al., Phys. Rev. Lett. **71**, 963 (1993).

	α (MeV)	β (MeV)	γ	δ (MeV)	$\varepsilon \left(\frac{c^2}{\text{GeV}^2}\right)$
S	-356	303	1.17	—	—
SM	-390	320	1.14	1.57	500
H	-124	71	2.00	—	—
HM	-130	59	2.09	1.57	500

TABLE I. Parametersets for the nuclear equation of state used in the IQMD model. S and H refer to the soft and hard equations of state, M refers to the inclusion of momentum dependent interaction.

$x = \sqrt{s}$ (GeV)	a (fm)	b
$2.104 - 2.12$	$294.6\,(x - 2.014)^{2.578}$	$19.71\,(x - 2.014)^{1.551}$
$2.12 - 2.43$	$\frac{0.01224}{(x-2.225)^2+0.004112}$	$19.71\,(x - 2.014)^{1.551}$
$2.43 - 4.50$	$(2.343/x)^{43.17}$	$33.41\,\arctan(0.5404\,(x - 2.146)^{0.9784})$

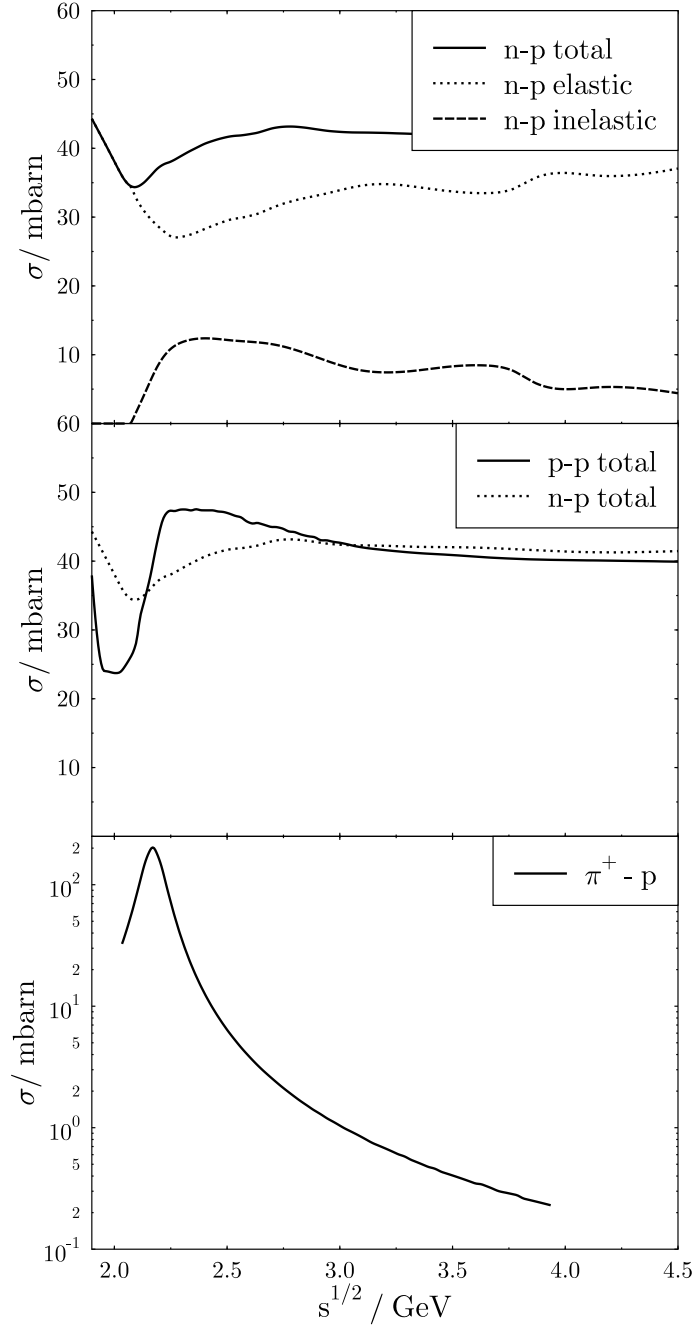TABLE II. $a(s)$ and $b(s)$ as functions of the c.m. energy.

FIG. 1. Tabulated cross sections in the IQMD model. The upper frame shows the total, elastic and inelastic proton neutron cross section. The middle frame compares the total proton neutron with the total proton proton cross section and the lower frame shows the total π^+ proton (or π^- neutron) cross section. The other pion nucleon cross sections are determined by scaling the π^+ proton cross section either with 1/3 (π^+ neutron and π^- proton) or with 2/3 (π^0 neutron and π^0 proton).
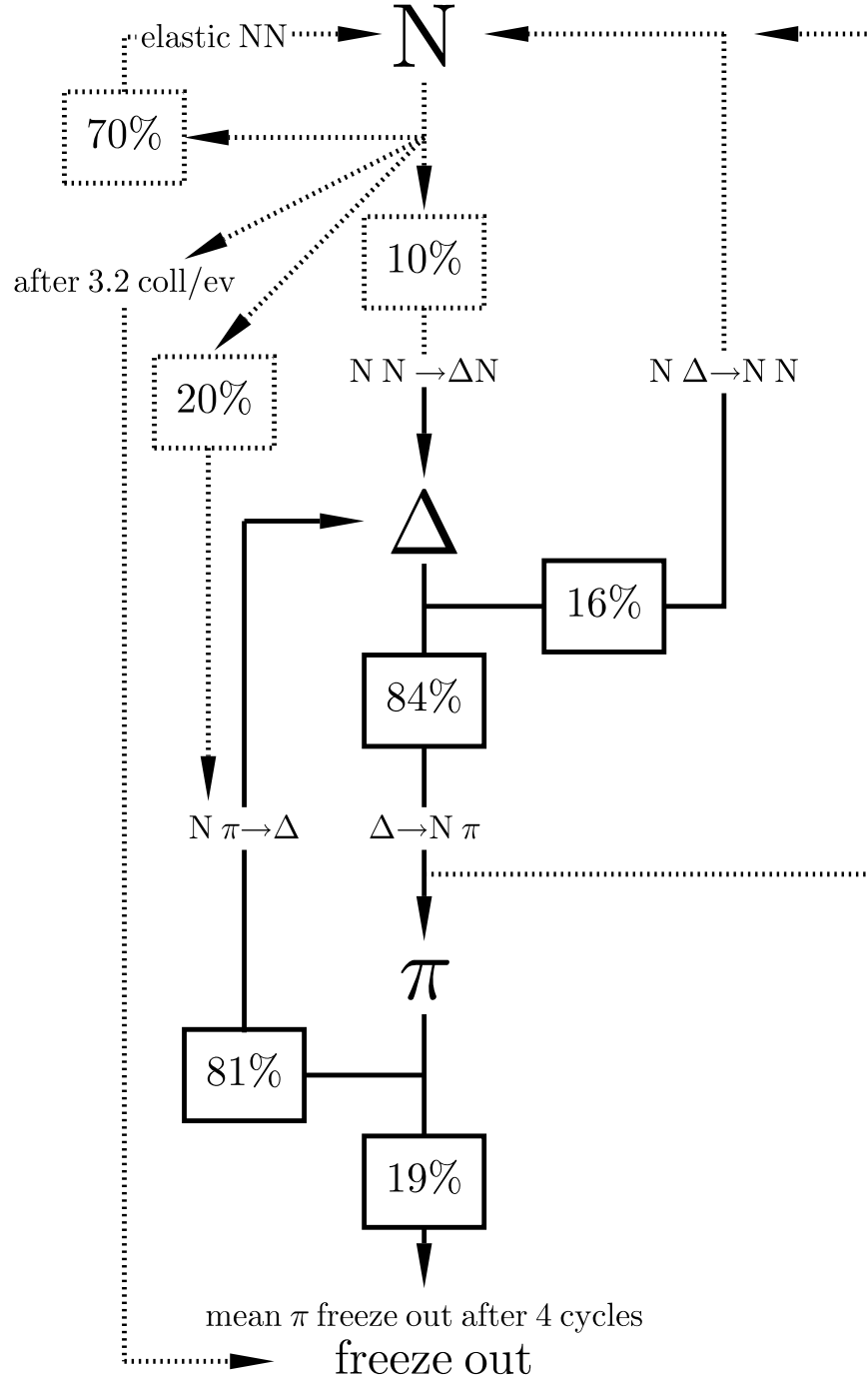
FIG. 2. Pion - nucleon cycle in the IQMD model. The scheme describes (for b ≤ 5 fm and time-averaged) all in the model possible processes linked to the creation of Δ-*matter*. The probabilities in the boxes always refer t o the vertices they are directly connected with. The main process for sustaining Δ-*matter* is the $\Delta \to N\pi \to \Delta$ loop, which, however, first has to be fueled by the $NN \to \Delta N$ process.

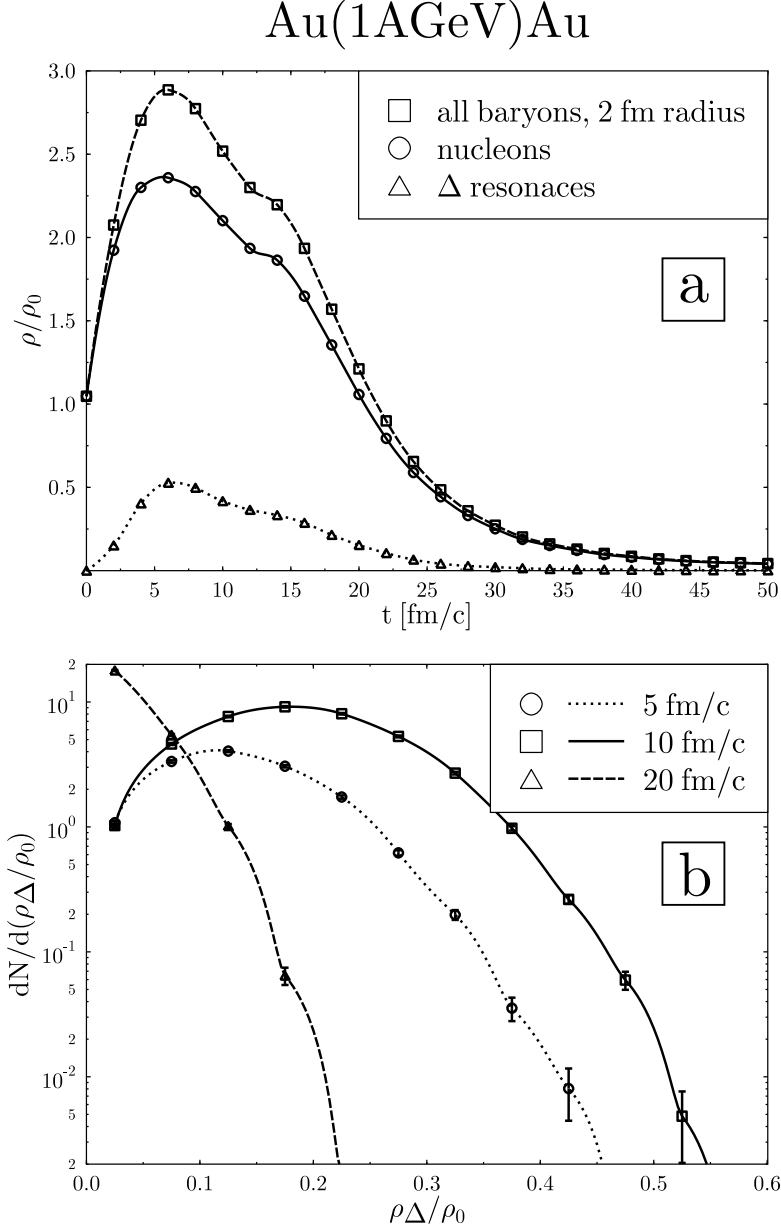FIG. 3. Time evolution of the the total baryon, nucleon and Δ-resonance density in units of ρ/ρ_0 (a) and Δ density distribution the respective Δs experience for 5, 10 and 20 fm/c. The densities in the upper frame (a) are calculated in a sphere of 2 fm radius around the collision center. The hot and dense reaction phase lies between 5 and 20 fm/c during which approximately 10% of the nucleons are excited to Δ-resonances. Up to 50% nucl. matter ground state density is reached by the Δ-resonances. However, less than 1% of the Δs experience such high densities. The average Δ density which is *felt* by the Δs is approximately 0.25 ρ_0 at 10 fm/c. The densities in the lower frame (b) were calculated by summing over all contributing Gaussians of all Δ's in the system at the locations of the respective Δ's.
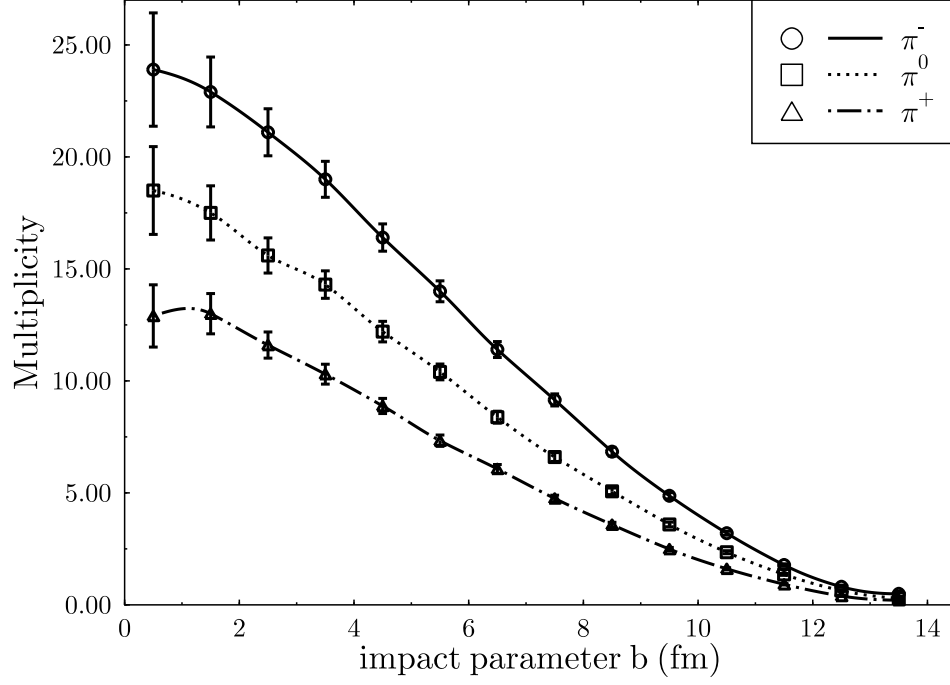
FIG. 4.   Multiplicity of π^-, π^0 and π^+ versus impact parameter b for Au+Au collisions at 1 GeV/nucl. incident beam energy. A hard EoS with momentum dependent interaction is used. For central collisions ($b = 0$ fm) the total pion multiplicity is approximately 55. For a minimum bias impact parameter distribution the average pion multiplicity is about 19 (8 π^-, 6 π^0 and 5 π^+).

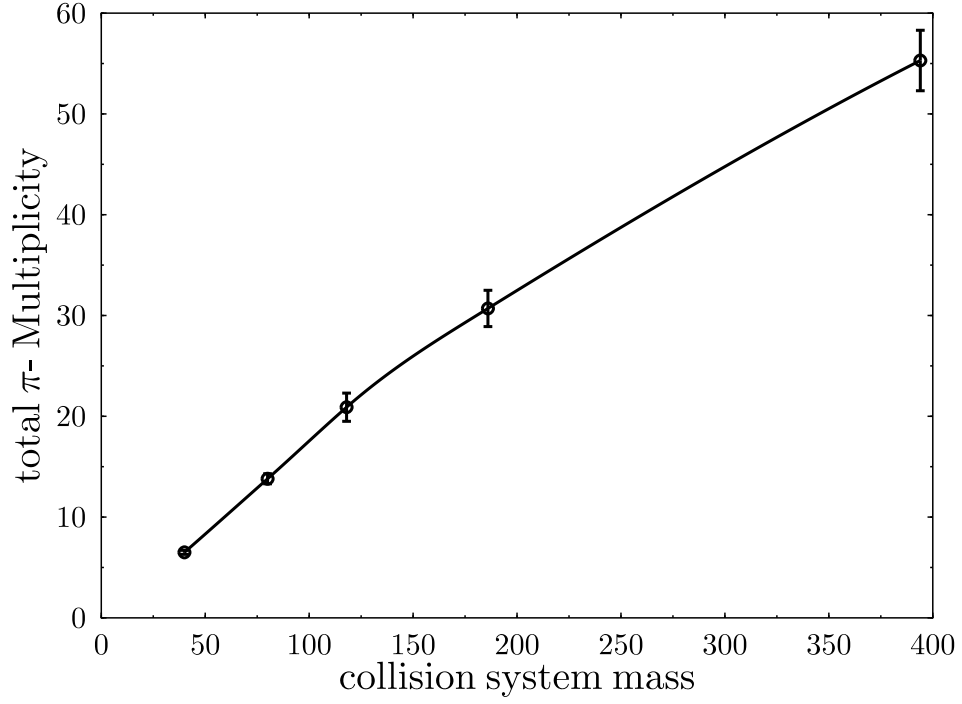FIG. 5. Total pion multiplicity versus collision system mass at 1 GeV/nucl. beam energy. For light collision systems the multiplicity increases linearly with the system mass. However, for heavy systems the increase is less than linear due to pion absorption. The values plotted were extracted from $b = 0$ fm calculations of the systems Ne+Ne, Ca+Ca, Ni+Ni, Nb+Nb and Au+Au.
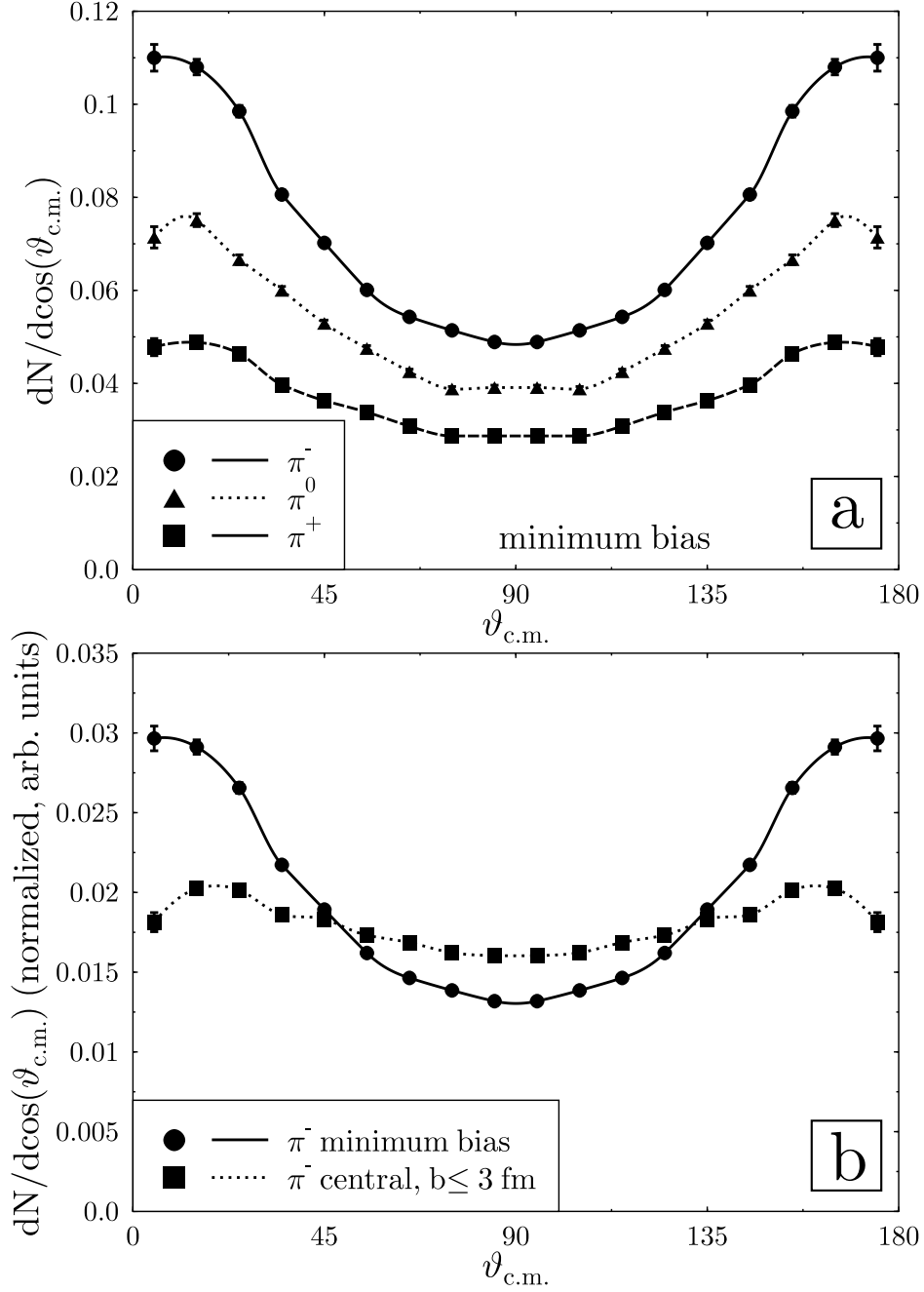
FIG. 6. Polar angular distribution $\frac{dN}{d\cos\vartheta_{c.m.}}$ for π^-, π^0 and π^+ in minimum bias (a) and for pi^- in minimum bias and central (b) Au+Au collisions. A horizontally flat distribution would correspond to an isotropic emission. For minimum bias events (top) a strong peaking towards forward–backward angles is observed, most prominently for π^-. The anisotropy decreases when studying central collisions (bottom). It can be explained by the decay of Δ-resonances in the projectile- and target- spectator regions.

FIG. 7.   Comparison of inclusive π^0 spectra $\frac{d\sigma}{p_t dp_t}$ for Au+Au and Ca+Ca (minimum bias) collisions between the IQMD model and data measured by the TAPS collaboration. A hard EoS including momentum dependence is used and a rapidity cut according to the acceptance of the TAPS spectrometer is employed. The model shows reasonable agreement with the heavy system Au+Au but it overpredicts the π^0 yield of the light system Ca+Ca by approximately 60%. The yield of low p_t pions in the heavy system is underpredicted by 10%.

FIG. 8.   Inclusive π^- and π^+ spectra $\frac{d\sigma}{p_t dp_t}$ for Au+Au (minimum bias) collisions at 1 GeV/nucl. as calculated with the IQMD model and a π^+ spectrum measured by the KaoS collaboration. A hard EoS including momentum dependence is used in the IQMD calculation and a rapidity cut according to the acceptance of the TAPS spectrometer is employed; the KaoS measurement has been acceptance-corrected. The slope of the π^+ spectrum in the model calculation agrees well with the KaoS measurements. However, the multiplicity as predicted by the model is approximately 20% above the KaoS measurements.

FIG. 9.   Ratio of the pion yield from Au+Au and Ca+Ca collisions plotted versus the transverse momentum p_t. The figure shows a comparison between data measured by the TAPS collaboration and an IQMD calculation (minimum bias, hard equation of state with momentum dependence). For low transvere momenta the model underpredicts the data approximately by a factor of 2.

FIG. 10. π^- to π^+ ratio versus transverse momentum p_t for Au+Au collisions (minimum bias) at 1 GeV/nucl. with a hard EoS and momentum dependence. The solid line shows the full calculation including Coulomb forces. For high p_t the ratio decreases towards 1 whereas for low p_t it increases to 2.5 – considerably higher than the value of 1.8 which the Δ-isobar model would suggest. The dashed line shows a calculation without Coulomb forces acting upon the pions. Within the errorbars the ratio remains constant at a value around 1.8.

FIG. 11.   Rapidity y vs. $\vec{p_x}/m$ for π^+ and protons in Au+Au collisions at 1 GeV/nucl. with minimum bias impact parameter distribution and a hard EoS including momentum dependence. The protons show the expected bounce-off. The $\vec{p_x}$ of the pions is directed oppositely to that of the protons. This effect is caused by rescattering of pions from large chunks of spectator matter.

FIG. 12.   in–plane transverse momentum $\vec{p_x}$ versus rapidity y (in the c.m. system) for π^+ in central Au+Au collisions with impact parameters b≤ 3 fm. Calculations with a hard equation of state without momentum dependence (squares), the same equation of state with momentum dependence (circles) and a CASCADE calculation (triangles) are shown. The effect of the momentum dependence is considerable, exhibiting the sensitivity of $\vec{p_x}$ on the baryon flow. The CASCADE calculation gives a different phase space distribution due to its lack of collective baryon flow.

FIG. 13. p_x^{dir} versus impact parameter b for Au+Au collisions at 1 GeV/nucl. with hard and soft equations of state, both with momentum dependence, and for the CASCADE calculation. Note the clear sensitivity for the equation of state on p_x^{dir}. The CASCADE calculation exhibits an anticorrelation between pions and nucleons for the whole impact parameter range, due to pion nucleon scattering and its lack of collective baryon flow.

FIG. 14.   Normalized azimuthal angular distribution $dN/d\varphi$ for π^0 with low and high transverse momentum p_t at mid-rapidity in the reaction Au(1AGeV)Au with minimum bias impact parameter distribution, a hard equation of state and momentum dependent interaction. The points were fitted according to the function $a \cdot (1 + b \cdot \cos(\phi) + c \cdot \cos(2\phi))$. The maximum at $\varphi = 90°$ corresponds to a preferential emission of high p_t pions perpendicular to the reaction plane. This is due to pion absorption by large pieces of baryonic spectator matter located predominantely in the reaction plane. Perpendicular to the plane there is no such spectator matter and pions with high p_t can leave the reaction zone without further interaction. Low p_t pions have rescattered more often which is only possible in the reaction plane. The inlay shows data from the TAPS collaboration for the region 400 MeV $\leq p_t \leq$ 600 MeV and midrapidity.

FIG. 15.   Squeeze-out ratio $R_{out/in}$ versus transverse momentum p_t for π^+ and π^-. Pions with $p_t \geq 200$ MeV are preferentially emitted perpendicular to the reaction plane. Pions with $p_t \leq 100$ MeV are emitted isotropically because they have undergone frequent rescattering which can only happen due to spectator matter in the reaction plane. The differences between π^- and π^+ are due to Coulomb forces. The inlay shows data on π^+ from the KaoS collaboration.

FIG. 16.   Distribution of the number of delta generations n_Δ a pion goes through before its freeze out for π^+ emitted in the reaction plane and perpendicular to it. 90% of the produced pions scatter at least once before leaving the reaction zone. The observed preferential emission perpendicular to the reaction plane is due to an excess of pions which on the average have undergone fewer collisions (≤ 2) than the pions in plane.

FIG. 17.   Azimuthal angular distribution $dN/d\varphi$ for neutral pions calculated with hard and soft equations of state (both with momentum dependence) and a CASCADE calculation.   All calculations were performed with an impact parameter of b=6 fm. Both equations of state exhibit approximately the same angular distribution whereas the CASCADE calculation does not exhibit any peak perpendicular to the event plane.   For larger impact parameters, however, also the CASCADE calculation shows a pronounced *squeeze–out*.

FIG. 18.   *squeeze–out ratio* $R_{out/in}$ versus impact parameter for neutral pions. The calculations were performed with the hard equation of state with (circles) and without (squares) momentum dependence as well as in CASCADE mode (triangles). Cuts around mid-rapidity ($-0.2 \leq y_{c.m.} \leq 0.2$) and for high transverse momentum ($p_t \geq 300$ MeV) were employed. For large impact parameters the CASCADE calculation agrees with the hard equation of state without momentum dependence. However, the onset of *squeeze–out* in CASCADE mode is shifted towards larger impact parameters in comparison with the hard equation of state. Most importantly, the inclusion of the momentum dependence results in a drastic increase of the *squeeze–out ratio*. The lines are inserted to guide the eye.